JOURNAL OF AGRICULTURAL AND FOOD CHEMISTRY

Kinetic Analysis of Nonisothermal Differential Scanning Calorimetry of 1,3-Dipalmitoyl-2-oleoylglycerol

KEVIN W. SMITH,*,† FRED W. CAIN,‡ AND GEOFF TALBOT§

Life Science, Unilever R&D Colworth, Sharnbrook, Bedfordshire, MK44 1LQ, United Kingdom, Loders Croklaan BV, Postbus 4, 1520 AA Wormerveer, The Netherlands, and The Fat Consultant, Suite 250, St Loyes House, 20 St. Loyes Street, Bedford, Bedfordshire, MK40 1ZL, United Kingdom

The crystallization of fats has been extensively studied because of its importance in the processing of food and food ingredients. Differential scanning calorimetry (DSC) is widely used in such studies. The aim of this study was to examine the determination of kinetic parameters from nonisothermal DSC crystallization of a model fat, 1,3-dipalmitoyl-2-oleoylglycerol. We applied peak and isoconversional methods to determine activation energies and compared these techniques with a nonparametric method, which separates the temperature dependence and degree of crystallization dependence of the crystallization rate. The Johnson−Mehl−Avrami−Erofeyev−Kolmogorov (JMAEK) model provided the best fit to the data, while the temperature dependence of the rate constant was best explained by a Vogel−Fulcher relationship, where the reference temperature was the melting point of the crystallizing species.

KEYWORDS: POP; DSC; differential scanning calorimetry; crystallization; nucleation; crystallization model; activation energy; nonisothermal crystallization; nonparametric kinetic analysis; Avrami; Vogel−Fulcher; isoconversional

INTRODUCTION

The crystallization of fats is important in the processing of many food products including chocolate, ice cream, and margarine or spread. In addition, it is highly significant in the fractionation of fats and oils, where products of varying physical properties are generated by crystallization and separation. For this reason, many researchers have studied the crystallization of oils and fats. Timms (*1*) and Sato et al. (*2*), for example, note the relevance of the crystallization kinetics to fat production.

Many studies have compared the crystallization of different fats. Chen et al. (*3*) have examined palm oil. The effect of nontriacylglycerol (non-TAG) components has also been explored. Wright and Marangoni (*4*), for example, have reported the effect of diacylglycerols on the crystallization of milk fat by pulse NMR. Various kinetic models have been applied in an attempt to characterize fat crystallization and enable a simpler comparison than comparing several sets of crystallization data (*5*). Many techniques have been applied in fat crystallization studies (*6*), including microscopy (*7*), pulse nuclear magnetic resonance (pNMR) (*4*), differential scanning calorimetry (DSC) (*8*), ultrasound (*9*, *10*), and X-ray diffraction (*11*, *12*).

Beyond measuring the crystallization of fat, it is desirable to be able to form a model that can be used to predict the crystallization of fat. Over the last 2 or 3 decades, attempts have been made to mathematically model the isothermal crystallization of fats to provide a quantification of their crystallization behavior. Rousset (*13*) has provided a good overview of modeling the crystallization of TAGs, as have Foubert et al. (*5*).

The most popular among the kinetic models applied to fats has been the Avrami model, also developed independently by other workers and thus referred to as the Johnson−Mehl−Avrami−Erofeyev−Kolmogorov (JMAEK) model (*14*, *15*, *16*, *17*, *18*, *19*). Other models applied to fats include that of Gompertz (*20*) and, more recently, that developed by Foubert et al. (*21*).

DSC has been widely used in the study of crystallization of many materials, including fats (*22*, *23*, *24*, *25*). Using this technique, crystallization may be studied isothermally or nonisothermally. In the isothermal method, the molten sample is cooled rapidly to a temperature below the freezing point and the progress of the crystallization is monitored as a function of time. This method has the advantage that the temperature-dependent factors are invariant, and the crystallization rate is dependent only on the degree of crystallization. However, it has the disadvantage of being sensitive to the temperature. If the temperature is too high, the crystallization rate will be low and the DSC signal will be lost among baseline noise or, at best, be distorted. Additionally, the crystallization could take a long time to complete. If the temperature is too low, the crystallization rate may be so high that the sample will begin to crystallize even before the required isothermal temperature has been

* To whom correspondence should be addressed. Telephone: +44 1234 222786. Fax: +44 1234 222552. E-mail: kevin.w.smith@unilever.com.
† Life Science.
‡ Loders Croklaan BV.
§ The Fat Consultant.

10.1021/jf048036o CCC: $30.25
Published on Web 03/23/2005

reached and the beginning of crystallization will be lost in the starting/stopping transient of the instrument. It can take some time to find suitable temperatures between these two extremes, and the temperature range may not be wide. To determine the temperature dependence, crystallization is carried out at several temperatures, preferably over as wide of a range as possible.

In the nonisothermal method, the molten sample is cooled, at a constant rate, through the melting point and beyond. This allows the crystallization to be recorded within a reasonable time, and there is no need to search for a suitable temperature range. Data are collected at several cooling rates. Using the nonisothermal method introduces a different problem, however: the crystallization rate is dependent on degree of crystallization and temperature, both of which are varying.

The use of DSC to study fat crystallization kinetics is dependent on certain assumptions. First, there is no thermal gradient within the sample. The possibility of this is reduced with small sample sizes. Second, the heat flow is proportional to the crystallization rate. This is justified if the same molecule or class of molecules participates throughout the crystallization.

In the majority of studies in which the crystallization of fat is modeled, isothermal crystallization is measured, often at a number of temperatures. Studies of nonisothermal crystallization have usually been comparative in nature with no application of a kinetic model.

It was the aim of the present study to examine the application of kinetic analysis to nonisothermal fat crystallization. Among fats, cocoa butter has been widely studied because of its importance in chocolate and confectionery. Palm oil has also been extensively studied. In this work, a principal TAG common to these fats was selected as a simple model system. Pure 1,3-dipalmitoyl-2-oleoylglycerol (POP) has been crystallized at various cooling rates using DSC. The data have been analyzed by a number of methods that aim to extract kinetic parameters. Popular methods based on the peak, such as the Kissinger method, are compared with isoconversional techniques such as that of Vyazovkin (for example, see ref *26*). The latter assumes a model for temperature dependence (Arrhenius) but does not depend on any specific kinetic model; it permits a calculation of the effective activation energy as a function of the degree of conversion.

The data were also analyzed using the nonparametric kinetics (NPK) method of Serra et al. (*27*, *28*). This makes no assumptions regarding the dependence of the crystallization rate, either on the temperature or on the degree of conversion, but separates these factors from the nonisothermal data. Once this was achieved, the dependence on the degree of conversion and on the temperature could be analyzed individually.

THEORY

The expression for the rate of a simple reaction (including crystallization) can be given by

$$\frac{d\alpha}{dt} = f(\alpha)g(T) \tag{1}$$

where $f(\alpha)$ represents the kinetic model of the process and $g(T)$ accounts for the temperature dependence of the reaction rate.

The kinetic model is often derived from the JMAEK equation, here as presented by Khanna and Taylor (*29*)

$$\alpha = 1 - \exp(-(Kt)^n) \tag{2}$$

where n is the Avrami exponent, dependent on the mode of nucleation and crystal growth, and K is the temperature-dependent rate constant [in the original Avrami equation, K was not raised to the power n, leading to a dependence of the rate constant on the exponent (*29*)]. $f(\alpha)$, in this case, is given by

$$f(\alpha) = n(1-\alpha)[-\ln(1-\alpha)]^{((n-1)/n)} \tag{3}$$

In common with many others, this model does not distinguish between nucleation and crystal growth.

In the case of the JMAEK equation, $g(T) = K$, where K is usually represented by the Arrhenius equation

$$g(T) = K = A\exp\left(-\frac{E_a}{RT}\right) \tag{4}$$

where R is the universal gas constant, A is the pre-exponential factor, and E_a is the activation energy. In the case of the crystallization process, the activation energy is apparent only, because it incorporates the activation energies for both nucleation and crystal growth.

Several methods have been used to obtain kinetic parameters from nonisothermal experiments carried out at different heating rates. They depend on the determination of the activation energy in a previous stage. There are three popular methods for the determination of the activation energy from differential thermal data. All make use of the peak temperature (temperature at the maximum rate or maximum heat flow), which will vary with the heating rate. First, the Kissinger method (*30*)

$$\ln\left(\frac{\beta}{T_p^2}\right) = \ln\left(-\frac{RA}{E_a}f'(\alpha_p)\right) - \frac{E_a}{R}\frac{1}{T_p} \tag{5}$$

where β (in K/min) is the heating rate, T_p (in K) is the temperature at the peak (maximum reaction rate), α_p is the degree of transformation at the peak temperature, and $f'(\alpha)$ is the derivative of $f(\alpha)$.

Second, the Ozawa method, as applied to maximum points (*31*, *32*)

$$\ln(\beta) = C - 1.052\frac{E_a}{R}\frac{1}{T_p} \tag{6}$$

where C is a constant that incorporates the Arrhenius pre-exponential factor, A, and the degree of crystallization function, $f(\alpha)$.

Third, the peak heights method of Kaiser and Ticmanis (*33*)

$$\ln(P) = \ln[Cf(\alpha_p)] - \frac{E_a}{R}\frac{1}{T_p} \tag{7}$$

where P is the peak height normalized by dividing by the sample weight and C is a constant proportional to the Arrhenius pre-exponential factor. Note that eqs 5 and 6 make use of the scanning rate.

The temperature scanning rate, β, is positive when heating and negative when cooling. This means that it is impossible to calculate $\ln(\beta)$ for cooling experiments. Some workers have attempted to apply the methods simply by neglecting the sign of the scanning rate. However, Vyazovkin (*34*) has clearly shown that this is not valid, because this neglects other conditions of sufficiency. Nevertheless, the calculations will be applied to the experimental data presented here, to illustrate the magnitude of the errors.

The above methods plot the left-hand side of the equation against the reciprocal of the peak temperature, yielding the

activation energy, E_a, as part of the determined slope of a straight line through the data points.

During crystallization, more than one process takes place (see chapters 5 and 6 in ref *35*). The initial step is nucleation (which may continue throughout the crystallization period) followed by crystal growth. The observed rate constant, $K_{overall}$ will be a combination of the rate constants for these two processes

$$\frac{1}{K_{overall}} = \frac{1}{K_{nucleation}} + \frac{1}{K_{growth}} \tag{8}$$

Crystal growth is itself composed of various steps, with the principal ones being diffusion of the molecule to the crystal surface and integration of the molecule into the crystal structure. Again, each of these processes has its own rate constant. Thus, the observed rate constant is a combination of rate constants from several different processes. As crystallization progresses, the relative contribution of these different processes to the overall rate constant may change, leading to a change in the effective apparent activation energy.

Isoconversional techniques attempt to determine the variation in apparent activation energy as a function of the degree of conversion. They rely on the fact that equal degrees of conversion lead to identical values of the kinetic function, $f(\alpha)$. The benefit of this is that changes in the reaction mechanism as a function of the degree of conversion can be exposed. Examples of these methods are the Friedman method (*36*)

$$\ln\left(\frac{d\alpha}{dt}\right) = \ln[Af(\alpha)] - \frac{E_{a,\alpha}}{R}\frac{1}{T_\alpha} \tag{9}$$

and the Ozawa method generalized to be isoconversional

$$\ln(\beta) = C - 1.052\frac{E_{a,\alpha}}{R}\frac{1}{T_\alpha} \tag{10}$$

where T_α is the temperature and $E_{a,\alpha}$ is the apparent activation energy at degree of crystallization α. Vyazovkin has proposed an alternative isoconversional method (*37*, *38*).

Vyazovkin's method necessitates the minimization of the function $\Phi(E_{a,\alpha})$

$$\Phi(E_{a,\alpha}) = \sum_{i\neq j}^{n}\sum^{n}\frac{J[E_{a,\alpha},T_i(t_\alpha)]}{J[E_{a,\alpha},T_j(t_\alpha)]} \tag{11}$$

where $T_i(t_\alpha)$ ($i = 1, ..., n$) is the temperature variation, n is the number of scanning rates, t_α is the time at degree of crystallization α, and function J is defined as

$$J[E_{a,\alpha},T_i(t_\alpha)] = \int_{t_\alpha-\Delta\alpha}^{t_\alpha}\exp\left[-\frac{E_{a,\alpha}}{RT_i(t_\alpha)}\right]dt \tag{12}$$

where $T_i(t_\alpha)$ is the temperature at time t_α and $\Delta\alpha$ depends on the number of steps chosen for analysis between $\Delta\alpha$ and $1 - \Delta\alpha$.

Substituting the time for which a given degree of crystallization has occurred, t_α, and the actual temperature at that moment into eq 12 and varying $E_{a,\alpha}$ until a minimum is achieved yields an estimate of the activation energy. Repeating this for different degrees of crystallization, α, shows how the apparent activation energy varies as crystallization progresses.

Li and Tang (*39*, *40*) derive an isoconversional method that does not include any approximations. They take logarithms of both sides of the rate equation (eq 1) where $g(T)$ is the Arrhenius dependency to yield the following equation:

$$\int_0^\alpha \ln\left(\frac{d\alpha}{dt}\right)d\alpha = -\frac{E_{a,\alpha}}{R}\int_0^\alpha\frac{d\alpha}{dT} + G(\alpha) \tag{13}$$

where

$$G(\alpha) \equiv \alpha\ln(A) + \int_0^\alpha \ln(f(\alpha))d\alpha \tag{14}$$

and has the same value for isoconversion points, irrespective of the cooling or heating rate. The two integrals in eq 13 are evaluated numerically from the data at each degree of conversion, α, for each scanning rate. A least-squares linear fit to the points yields a slope equal to $-E_{a,\alpha}/R$.

All of the above methods assume an Arrhenius temperature dependency. A modified Arrhenius model, the Vogel−Fulcher equation, includes a third parameter that effectively references the temperature to a constant temperature, T_0

$$g(T) = A\exp\left(-\frac{E}{R(T-T_0)}\right) \tag{15}$$

and can be applied in cases of crystallization (ref *41* and, similarly, ref *42*; also see refs *43* and *44*) from supercooled melts above the glass transition temperature, where the dominant process is diffusion-controlled. It should be noted that A and E in eq 15 are not the pre-exponential factor or activation energy as classically understood from the Arrhenius equation. Replacing T with $(T - T_0)$ in each of the above equations (*5*, *6*, *7*, *9*, *10*, *11*, and *13*) allows for a Vogel−Fulcher temperature dependency.

There are many kinetic models to describe the variation in crystallization rate with the degree of crystallization. These include the popular JMAEK model, eq 3, which is a special case of the Šesták−Berggren equation (*45*, *46*)

$$\frac{d\alpha}{dt} = K\alpha^m(1-\alpha)^n[-\ln(1-\alpha)]^p \tag{16}$$

The JMAEK equation arises when $m = 0$ and $n = 1$ (note, n in eq 16 is not the same as the Avrami exponent). Other commonly applied models also arise from eq 16, for example, the two-parameter model of Nomen and Sempere (*28*) appears when $p = 0$

$$\frac{d\alpha}{dt} = K\alpha^m(1-\alpha)^n \tag{17}$$

The Gompertz equation, although more commonly applied to microbial growth, has been applied by Kloek et al. (*20*) and Vanhoutte et al. (*47*) to the crystallization of fats and may be presented as

$$\alpha = \exp(-\exp(\mu e(\lambda - t) + 1)) \tag{18}$$

where λ is the induction time, μ is the maximum rate of crystallization, e is Euler's constant (2.7182), and the maximum degree of crystallization has been taken as equal to 1. This must be derivatized and substituted for t to yield the kinetic function, $f(\alpha)$

$$f(\alpha) = \mu e\alpha[-\ln(\alpha)] \tag{19}$$

Finally, Foubert et al. (*21*) have presented a model based on a first-order forward reaction and an nth order reverse reaction

$$\frac{dh}{dt} = K_n h^n - K_1 h \quad (20)$$

where K_n and K_1 are rate constants, $h = (1 - \alpha)$, α is the degree of crystallization, and α as $t \rightarrow \infty$ is 1. This is a special case of the equation of Karkanas et al. (*48*, *49*), which was itself derived from that of Kamal (*50*). Parameter estimation studies showed that K_1 and K_n differed only little, hence the model was simplified to

$$\frac{dh}{dt} = K(h^n - h) \quad (21)$$

Putting this in terms of α, as with other models, yields

$$\frac{d\alpha}{dt} = K((1 - \alpha) - (1 - \alpha)^n) \quad (22)$$

which yields the kinetic function

$$f(\alpha) = ((1 - \alpha) - (1 - \alpha)^n) \quad (23)$$

Clearly, it would be advantageous to separate $f(\alpha)$ and $g(T)$ from the data without making any assumptions regarding the specific form of the functions. The crystallization rate at any point is dependent only on the degree of conversion, α, and the temperature, T, according to eq 1. Note that no consideration is made of the history of the system, making the crystallization rate solely dependent on degree of crystallization and temperature. Thus, the crystallization rate may be represented in a three-dimensional space as a surface of crystallization rate plotted against the temperature and degree of crystallization, which can be analyzed by the NPK method described by Serra et al. (*27*, *28*). This method permits the separation of the temperature and the degree of conversion functions from the experimental data. Full details can be found in their papers and also is explained clearly by Sewry and Brown (*51*). The approach is summarized here.

The surface of crystallization rate against the temperature and degree of crystallization can be discretized and represented as an ($n \times m$) matrix, **A** (note that matrixes are given in bold uppercase), where

$$\mathbf{A} = \begin{pmatrix} f(\alpha_1)g(T_1) & f(\alpha_1)g(T_2) & \cdots & f(\alpha_1)g(T_m) \\ f(\alpha_2)g(T_1) & f(\alpha_2)g(T_2) & \cdots & f(\alpha_2)g(T_m) \\ \vdots & \vdots & \vdots & \vdots \\ f(\alpha_n)g(T_1) & f(\alpha_n)g(T_2) & \cdots & f(\alpha_n)g(T_m) \end{pmatrix} \quad (24)$$

where $f(\alpha_i)$ is the function of the degree of crystallization and $g(T_j)$ is the temperature-dependent function; columns correspond to different degrees of crystallization ($\alpha_1 - \alpha_n$), and rows correspond to different temperatures ($T_1 - T_m$), where $n \geq m$. Singular value decomposition (SVD) is used to decompose the matrix into the product of three matrixes (*52*)

$$\mathbf{A} = \mathbf{U}\mathbf{W}\mathbf{V}^T \quad (25)$$

where **U** and **V** are orthonormal matrixes and **W** is a diagonal matrix whose elements are the singular values of **A**. Provided that only the first singular value is significant (i.e., it is much larger than the other values), **A** can be expressed simply as the product of the first column of **U**, the first column of **V**, and the first singular value.

In practice, the whole of matrix **A** is not available and submatrixes must be selected from the data. Each of these may be decomposed to yield two vectors accounting for the temperature and degree of crystallization. Because, by the nature of SVD, the singular values for each of these submatrixes will differ, the vectors will not be continuous from all submatrixes and each vector must be multiplied by a factor to bring them into concurrence. To find these factors, the adjacent submatrixes must be selected such that they overlap. The outcome of this process is the desired functions, $f(\alpha)$ and $g(T)$, whose form may be compared to chosen models to identify the most suitable kinetics.

Because the measured crystallization rate, $d\alpha/dt$, is a product of the degree of crystallization function, $f(\alpha)$, and the temperature function, $g(T)$, according to eq 1, we must determine in which order to analyze these functions. If either of these functions include a constant multiplier (as does the Arrhenius model, eq 4, which has the pre-exponential factor, A), this multiplier will be divided arbitrarily between the two vectors when calculating the SVD. If $g(T)$ but not $f(\alpha)$ includes a constant multiplier, the correct factor can be found by first fitting the desired kinetic equation to $f(\alpha)$ and extracting a constant scaling multiplier, which can be applied to $g(T)$. If both functions include a constant multiplier, then neither factor can be found, although other parameters may be determined.

MATERIALS AND METHODS

POP was synthesized in the Unilever Research Vlaardingen Laboratory and finally purified by preparative HPLC and crystallization from acetone. Analysis by FAME GC showed the POP having 66.7% C16:0 and 33.3% C18:1. TAG GC showed 99.6% C50 in the POP (C48, 0.1%; C52, 0.3%), while silver phase HPLC gave a value for symmetrical disaturated−monounsaturated TAG, SatOSat, of 99.9% (SatSatSat was 0.1%).

A Perkin−Elmer Pyris I DSC was utilized and was calibrated, at each rate used, with indium and β-naphthylethyl ether (melting point, 35 °C). Samples of TAG of approximately 10 mg were weighed in DSC pans. Samples were heated to 100 °C, where they were held for 2 min to ensure the absence of nuclei, before cooling at 50 °C/min to 50 °C. Samples were crystallized by cooling, at a constant rate, from 50 °C to −30 °C. Specific rates used were 2.5, 5, 7.5, 10, 12.5, 15, and 17.5 °C/min. The lower and upper limits for scanning rates were determined by the necessity to crystallize only one polymorph and to be sure to maintain full temperature control during cooling. After crystallization, after holding for 2 min at −30 °C, samples were reheated at a rate of 5 °C/min to 60 °C. Using the software supplied with the instrument, after normalization for sample weight, the peak temperatures and areas were calculated and the crystallization data (partial peak areas) were exported at intervals of 0.5% crystallization as a file containing the temperature, degree of conversion, and heat flow (curve height).

SOFTWARE

Peak temperature methods (eqs 5−7) were applied by tabulating the cooling rate (β), peak height (P), and peak temperature (T_p in K) in a spreadsheet (Excel 97). Linear regressions were performed to determine E_a using the built-in LINEST function.

The partial area data exported by the DSC software was imported into a spreadsheet (again, Excel 97) for further analysis. The curve height (heat flow) data were converted to the crystallization rate by dividing by the total peak area. Thus, it was possible, for each cooling rate, to present a table of temperature (T) and crystallization rate ($d\alpha/dt$) against the degree of crystallization (α). Built-in functions were used to implement the methods of Ozawa, Friedman (*36*), and Li and Tang (*40*). Bespoke macros were used to implement the method of Vyazovkin (*26*).

For NPK analysis, a spreadsheet was used to define the required submatrixes (*27*, *28*, *51*) and then to interpolate the

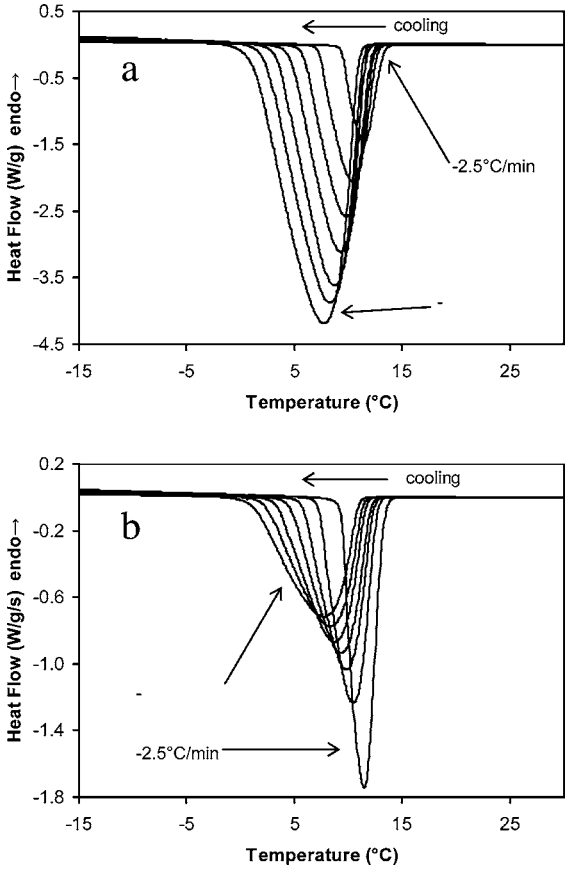

Figure 1. DSC crystallization curves of POP at scanning rates of –2.5, –5, –7.5, –10, –12.5, –15, and –17.5 °C/min. (a) Standard thermogram representation of normalized heat flow against temperature. (b) Normalized heat flow per second against temperature, illustrating that the peak areas are the same.

crystallization rate at set temperatures and degrees of crystallization to produce the matrixes necessary for SVD. SVD itself was carried out using a program specifically written for the purpose in Delphi Pascal (Borland Software Corporation), adapting the routines given by Press et al. (*52*) in their chapter 2.

Each of the kinetic models was fitted to $f(\alpha)$ using statistical software (JMP, SAS Institute Inc.), with the root-mean-squared error (RMSE) being used as a measure of fit. The same software was used to fit the Arrhenius and Vogel−Fulcher models to $g(T)$.

As a final check on the parameters obtained from the NPK method, a program was written in Delphi Pascal to calculate crystallization curves from the parameters (n, A, E_a, and T_0) using the Runge−Kutta method, again adapting routines from Press et al. (*52*) in their chapter 15.

RESULTS AND DISCUSSION

Figure 1 shows the DSC thermograms collected at the different cooling rates. Note that the apparent area of the peak appears to increase with the cooling rate when the heat flow is presented, as it is here, as a function of the temperature rather than time. Both the peak onset and peak position shift downward in temperature as the scanning rate increases. The onset is expected to shift because of the induction time for crystallization, while the peak position will shift because of both the induction time and crystallization rate.

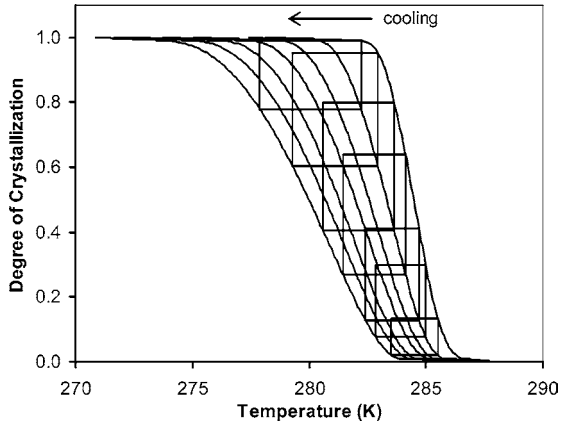

Figure 2. Integrated DSC crystallization curves of POP at scanning rates of –2.5, –5, –7.5, –10, –12.5, –15, and –17.5 °C/min. The overlapping submatrixes selected for the NPK analysis of Serra et al. (*27*, *28*) are shown as rectangles.

Table 1. Apparent Activation Energy Calculated by Peak Temperature Methods and Isoconversional Techniques

method type		Arrhenius E_a (kJ/mol)	Vogel–Fulcher[a] E_a (J/mol)
	Peak		
Kissinger	average	–352	–32
	standard error	–23	–2
Ozawa	average	–330	–110
	standard error	–22	–4
Kaiser and Ticmanis	average	–194	–64
	standard error	–13	–6
	Isoconversional		
Friedman	average	–172 (–147)[b]	–59 (–58)
	standard deviation	89	9
Ozawa	average	–124 (–119)	–46 (–47)
	standard deviation	37	10
Vyazovkin	average	–171 (–148)	–58 (–58)
	standard deviation	83	2
Li and Tang	average	–246 (–229)	–55 (–56)
	standard deviation	77	2

[a] T_0 (288.2 K) is taken as the average onset of the melting peak following each crystallization. [b] Value at 50% crystallization given in brackets.

Figure 2 shows the integral of the peaks presented in **Figure 1**, i.e., the degree of crystallization, as a function of the temperature. The peak area for all scanning rates was the same, 89.1 J/g (standard deviation of 2.77), which is the heat of fusion for the α polymorph [around 85 J/g according to Wesdorp, see table A1.7 in ref *53*, and 82 J/g according to Sato et al. (*54*)]. This agrees with the area found on subsequent melting of the same samples, 89.9 J/g (standard deviation of 3.03).

Table 1 lists the apparent activation energies determined by the peak temperature methods (eqs 5−7) by plotting the equations to determine the slope (which incorporates E_a). Unsurprisingly, the methods of Kissinger and Ozawa yield similar results, but the Kaiser and Ticmanis analysis gives a value only two-thirds as large. The standard error is similar in each case, being around 6.7%. These are based on the Arrhenius equation. However, if the Vogel−Fulcher versions of the equations are utilized, the figures for E_a are very different. Not only are they of a different order of magnitude, as would be anticipated, but the values vary widely, ranging from −32 to −110 J/mol. Standard errors also varied, between 3.9% (Ozawa) and 6.2% (Kissinger), but were lower (not significantly) than in the case of the Arrhenius model. For this analysis, T_0 in eq 15 was taken as the average onset of melting following

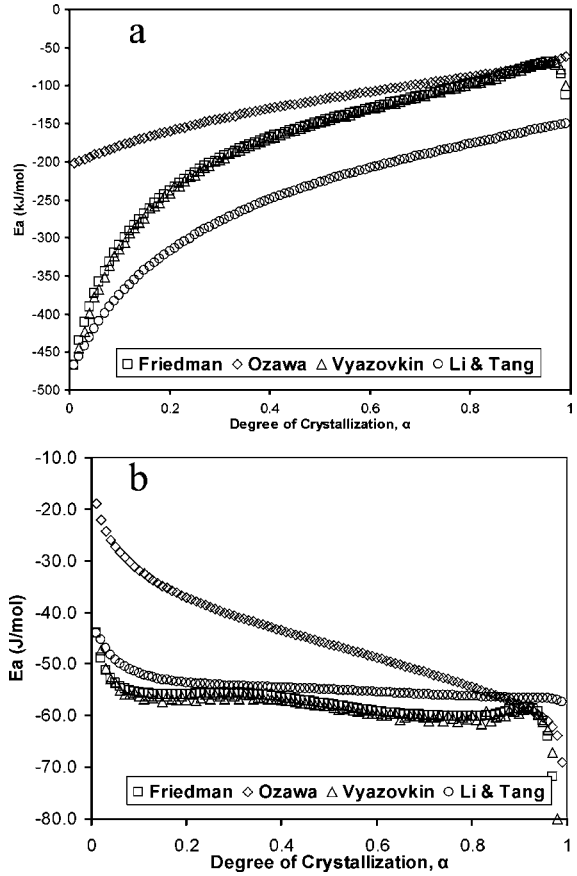

Figure 3. Variation in the apparent activation energy for crystallization of POP calculated using isoconversional methods. Temperature dependence assumed to be (a) Arrhenius or (b) Vogel–Fulcher.

crystallization at the different scanning rates, 288.22 K (standard deviation of 0.08), a reasonable figure to take given the outcome of the NPK analysis (see below). However, the temperature selected for T_0 has a large influence on the calculated energy. For example, a change of just 1 K can alter the calculated activation energy by 15−25 J/mol, depending on the method used, i.e., up to around 25% of the value of E_a. Thus, these methods are not suitable for the calculation of E_a when using the Vogel−Fulcher model because of the sensitivity to the value set for T_0.

Applying the isoconversional techniques (eqs 9−11 and 13) gives rise to the curves in **Figure 3**, which shows the apparent activation energy continuously varying throughout crystallization. It would be expected that the activation energy is invariant and indeed it should be. However, there are two situations in which the apparent (measured) activation energy may change. First, as described above, several processes (e.g., nucleation, diffusion, and surface integration) contribute, to a greater or lesser extent, to the overall process as crystallization progresses. Second, application of the wrong temperature dependency model can show continuously varying activation energy.

The average apparent activation energy from each method is presented in **Table 1**. For the Arrhenius temperature dependency, the Vyazovkin and Friedman methods gave an average figure similar to that from the Kaiser and Ticmanis peak method, but the Ozawa isoconversional technique yielded a somewhat smaller value and the Li and Tang method yielded a much larger value. Because of the wide variation in activation energy, the standard deviations were high (up to 50%). However, the average figures were similar to those found at the 50% crystallization point.

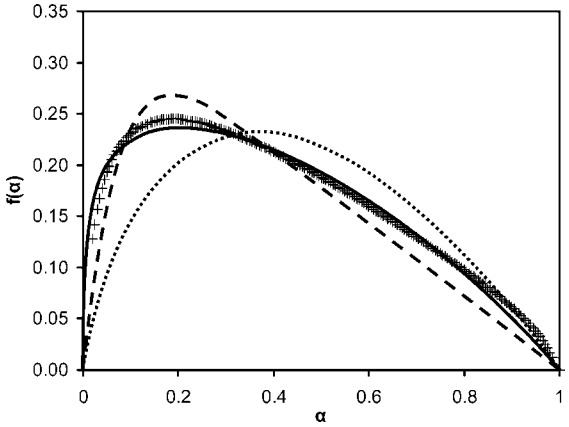

Figure 4. Degree of crystallization function, $f(\alpha)$, from the combined vectors obtained from the SVD of the submatrixes indicated in **Figure 2**. The figure shows data points (+) and the JMAEK (—), Foubert (- - -), and Gompertz (•••) kinetic models.

The curves of effective activation energy against the degree of crystallization are similar for the Friedman and Vyazovkin methods. All methods showed an apparent activation energy becoming less negative as α increases, with all but Ozawa showing sharper reductions in magnitude as α rose from zero than at higher levels of α (**Figure 3a**). The standard error on the calculation of each individual point was about 10% for all methods.

Using the Vogel−Fulcher temperature dependency (eq 15) gave rise to quite a different picture (**Figure 3b**). Ozawa showed the apparent activation energy becoming more negative with α, while the other three methods showed more or less constant and similar activation energy at around −55 to −60 J/mol. Standard deviations on these figures were smaller than in the case of Arrhenius dependency, as might be expected from the lower variation in apparent activation over the course of crystallization. Again, the sensitivity to the set value of T_0 means that these methods are not suitable for the determination of E_a, although they do indicate a trend in the activation energy. It is interesting to note that a presumption of the Arrhenius temperature dependency, for this process, leads to the conclusion that the apparent activation energy varies throughout the crystallization process, while use of Vogel−Fulcher dependency leads to an apparently constant activation energy (although not for the Ozawa approach).

The NPK method permits a separation of the temperature, $g(T)$, and degree of crystallization, $f(\alpha)$, dependence from the data before any evaluation of suitable models. Thus, following the method of Serra et al., the data was arranged in overlapping submatrixes as indicated in **Figure 2**. Each matrix was split by SVD, as described above.

The first singular value for each submatrix was found to be more than 2 orders of magnitude greater than any other singular value. Therefore, the temperature function, $g(T)$, and the degree of crystallization function, $f(\alpha)$, were taken as the first columns of the orthonormal matrixes, **U** and **V**. The correction factors were found by calculating the average factor across the overlapped portions of the matrixes for the degree of crystallization function, $f(\alpha)$. Note, again, that the calculated vectors can be used to calculate the crystallization rate at any temperature and degree of crystallization, without any need to analyze the functions further by interpolation between the vector points.

As noted previously, any constant multipliers in $f(\alpha)$ and $g(T)$ can be confounded. We made the reasonable assumption that the constant multiplier exists in the temperature-dependent

Table 2. Values of Parameters and RMSE for Fitted Kinetic Models

model		parameters[a]	value[b]	RMSE
Šesták–Berggren	$f(\alpha) = \alpha^m(1-\alpha)^n[-\ln(1-\alpha)]^p$	m	3.977 (0.180)	0.0042
		n	–0.554 (0.069)	
		p	–3.663 (0.176)	
		c	0.530 (0.007)	
JMAEK	$f(\alpha) = n(1-\alpha)[-\ln(1-\alpha)]^{((n-1)/n)}$	n	1.303 (0.006)	0.0075
		c	0.322 (0.001)	
Nomen–Sempere two parameter	$f(\alpha) = \alpha^m(1-\alpha)^n$	m	0.238 (0.007)	0.0072
		n	0.908 (0.012)	
		c	0.426 (0.006)	
Foubert	$f(\alpha) = ((1-\alpha) - (1-\alpha)^n)$	n	13.561 (0.521)	0.0195
		c	0.357 (0.004)	
Gompertz	$f(\alpha) = \mu e\alpha[-\ln(\alpha)]$	c	0.629 (0.010)	0.0401

[a] In fitting the experimentally determined function $f(\alpha)$, a constant scaling multiplier, c, is included for all models. This is later used as a correction factor for the experimentally determined $g(T)$. The Gompertz model is the only one which, of itself, includes a constant multiplier, μe, but this is confounded with the scaling multiplier for the temperature-dependence function, $g(T)$. [b] Approximate standard error given in brackets.

function (e.g., the Arrhenius pre-exponential factor, A), because a large number of models are formulated in this way. Thus, we first analyzed $f(\alpha)$, of which the data points are plotted in **Figure 4**.

The kinetic models described above (eqs 3, 16, 17, 19, and 23) were fitted to this experimentally determined $f(\alpha)$. It should be noted that the choice of kinetic model influences the derivation of the Arrhenius parameters (*51*).

Table 2 lists, for each model, the values of fitted parameters, their approximate standard errors, and the RMSE. The best fit was for the general Šesták−Berggren model (eq 16), but the fitted parameters were highly correlated (degree of correlation of 0.78 between n and c, rising to 0.99 between n and m or n and p). In addition, no mechanism has yet been proposed that would give rise to this equation. Only slightly worse fitting were the Nomen−Sempere two-parameter model (eq 17) and the JMAEK model (eq 3). The former also had highly correlated parameters (0.8 between n and m up to 0.95 between m and c), while the latter had one less parameter, with the remainder being uncorrelated (−0.27 between n and c), and should be preferred for this reason. The Foubert model (eq 23) fitted reasonably but not as well as the previously mentioned models, and the parameters were moderately correlated (−0.62 between n and c). The Gompertz model (eq 19) did not yield a good fit. Note that the calculated scaling multiplier, c, differs between the models. Because this will be used to correct the $g(T)$ vector, it is clear that the choice of kinetic model influences the value of the pre-exponential factor, A, although not of the apparent activation energy, E_a.

Because of the good fit and lack of correlation between the Avrami exponent and the fitted scaling multiplier, the JMAEK model seemed to be the most appropriate model. **Figure 4** shows the best-fit JMAEK line with the experimental data, along with the Foubert and Gompertz models. The value of the Avrami exponent is 1.3. When the data was fitted between 10 and 90% only, a much better fit was obtained (RMSE of 0.0044 compared with 0.0075), although the Avrami exponent differed only slightly, being 1.26.

Avrami exponents can theoretically range from 0.5 to 4 (*55*). A value of 0.5 would be characteristic of linear (rodlike) crystal growth and athermal (spontaneous) nucleation and rate-limited by diffusion. A value of 4 would indicate spherical growth and thermal (sporadic) nucleation and rate-limited by nucleation. The calculated exponent close to 1.5 could indicate two situations: either sporadic nucleation and linear growth with the rate limited by diffusion or spontaneous nucleation and spherical growth with the rate limited by diffusion. Because other factors may influence the obtained value of the exponent, assignment of a specific mode of crystallization is not possible without independent observation.

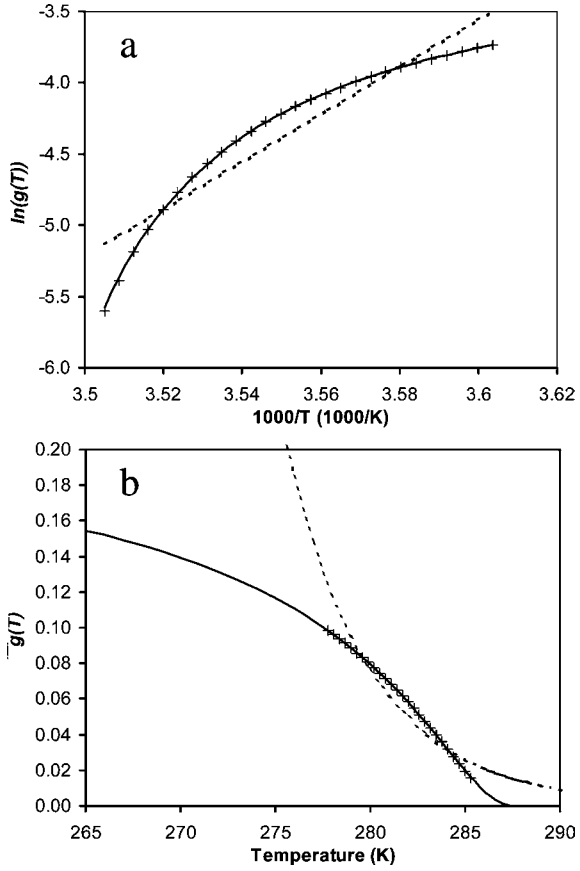

Figure 5. (a) Arrhenius plot of the temperature function, $g(T)$, from the combined vectors obtained from the SVD of the submatrixes indicated in **Figure 2**. The data (+) does not form a straight line; the best fit Arrhenius (- - -) is shown, along with the best-fit Vogel–Fulcher model (—). (b) Temperature function, $g(T)$, plotted against temperature (+). Extrapolations of the Arrhenius (- - -) and the Vogel–Fulcher (—) best fits are shown to illustrate the difference in behavior.

After a kinetic model was selected, the scaling multiplier, c, calculated from the parameter fitting was used to "correct" the temperature-dependent vector, $g(T)$, and the form of the temperature-dependent function was determined. From **Figure 5**, it is apparent that the dependence of K, i.e., $g(T)$, on temperature does not conform to an Arrhenius model. A standard Arrhenius

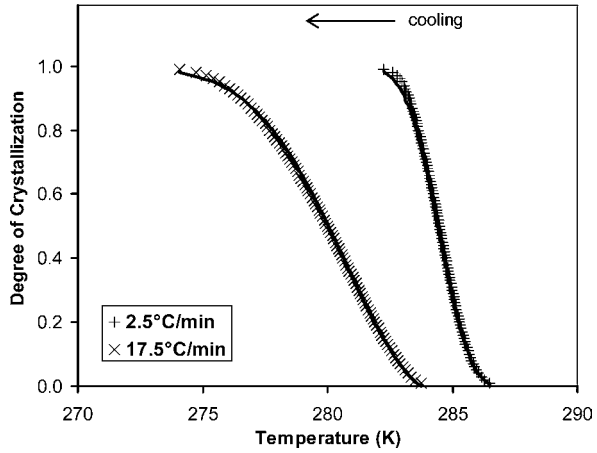

Figure 6. Calculated crystallization curves (—) with measured data (+ and ×) at slowest and fastest scanning rates.

plot (**Figure 5a**) does not show a straight line but is distinctly curved. In addition, the slope of the line is positive. The best-fit line had a RMSE of 0.0068, but the distribution of errors was not random. The line yielded a pre-exponential factor, A, of 1.79×10^{-28} s^{-1} and an apparent activation energy, E_a, of −142.7 kJ/mol. As might be anticipated, this is similar to the values found using the isoconversional methods (except that of Li and Tang).

The Vogel−Fulcher model, eq 15, fitted the data much better (RMSE of 0.00016). A fit of this equation to the data yielded a pre-exponential factor of 2.278×10^{-1} s^{-1} and an apparent activation energy of −76.7 J/mol (approximate standard error of 0.7 J/mol). Note that these figures are of quite a different order to those found using the Arrhenius model. The figure determined for the apparent activation energy is similar to that found from the isoconversional methods of Vyazovkin, Friedman, and Li and Tang (−55 to −60 J/mol). The fitted temperature constant, T_0, was 288.77 K (approximate standard error of 0.03 K) or 15.62 °C. This is very close to the melting point (as defined by the peak onset) determined by DSC when heating the samples following crystallization, which was 288.2 K (15.1 °C). Recalling the sensitivity of the calculation to T_0, when the figure calculated following NPK was used in the isoconversional methods, activation energies much closer to that found following NPK were obtained (−72.9, −67.7, and −72.4 J/mol from Friedman, Vyazovkin, and Li and Tang, respectively).

When the values were taken for the parameters fitted to the JMAEK and Vogel−Fulcher models, the DSC curves were calculated at the different rates as a check on the fitted parameters. It should be noted that no account has been made of induction times in the kinetic model. Although induction times can be accounted for in the JMAEK equation

$$\alpha = 1 - \exp(-K(t - t_i)^n) \qquad (26)$$

where t_i is the induction time, once eq 26 is differentiated and substituted for $(t - t_i)$, the function is the same as in eq 3. However, the shift necessary to overlay the calculated curves on the measured curves was found by initiating the calculated crystallization at a temperature (and hence, time) shifted downward from T_0, found by minimizing the sum of the squared errors between calculated and measured curves. When this was done, an excellent match was found between measured and calculated crystallization curves. Examples of the calculated curves are shown in **Figure 6**. The largest RMSE between calculated and measured data was 0.0019. The temperature shift from the apparent melting point, T_0, was translated into a pseudoinduction time. These times are shown in **Table 3**. However, these cannot be compared to conventional induction times because the temperature is not constant throughout the pseudoinduction time. As might be anticipated, the pseudoinduction time is longer at the slower scanning rates because more time is spent at higher temperatures.

Table 3. Pseudoinduction Times at Varying Scanning Rates

scanning rate (°C/min)	induction time (s)
−2.5	45.4
−5.0	35.3
−7.5	26.5
−10.0	20.1
−12.5	19.8
−15.0	17.6
−17.5	16.9

This study has demonstrated the application of NPK to the analysis of the nonisothermal crystallization of a pure TAG using DSC. Provided care is taken to ensure that the crystallizing polymorph is the same in each experiment; this technique enables the kinetic triplet [A, E_a, and $f(\alpha)$] to be determined. Ultimately, the conclusions made via this method concerning the kinetic model need to be confirmed with other techniques, such as microscopy. This study has employed a relatively simple system. Some TAG show more complicated DSC thermograms during crystallization (*56*). In addition, when mixtures of TAG are considered, as is the case with natural fats, the situation can be even more complex, perhaps involving crystallization of separate solid phases. Further consideration of the application to such systems of the methods presented here is necessary in the future.

ABBREVIATIONS USED

TAG, triacylglycerol; DSC, differential scanning calorimetry; HPLC, high-performance liquid chromatography; GLC, gas−liquid chromatography; FAME, fatty acid methyl ester; Sat, saturated; O, oleic; P, palmitic; JMAEK, Johnson−Mehl−Avrami−Erofeyev−Kolmogorov; NPK, nonparametric kinetics; SVD, singular value decomposition.

ACKNOWLEDGMENT

We thank Mr. B. S. Jeffrey, Mr. G. J. Sassano, and team for performing the GLC and HPLC analyses. Mr. K. M. Dilley prepared the samples for DSC and performed the experiments.

NOTE ADDED AFTER ASAP PUBLICATION

In the caption of Figure 5, the Arrhenius line is the dashed line and the Vogel−Fulcher line is the solid line. This paper was originally posted on the Web on March 23, 2005. The paper was reposted on the Web on April 4, 2005.

LITERATURE CITED

(1) Timms, R. E. Phase behaviour of fats and their mixtures. *Prog. Lipid Res.* **1984**, *23*, 1−38.
(2) Sato, K.; Ueno, S.; Yano, J. Molecular interactions and kinetic properties of fats. *Prog. Lipid Res.* **1999**, *38*, 91−116.
(3) Chen, C. W.; Lai, A. M.; Ghazali, H. M.; Chong, C. L. Isothermal crystallization kinetics of refined palm oil. *J. Am. Oil Chem. Soc.* **2002**, *79*, 403−410.
(4) Wright, A. J.; Marangoni, A. G. Effect of DAG on milk fat TAG crystallization. *J. Am. Oil Chem. Soc.* **2002**, *79*, 395−402.

(5) Foubert, I.; Dewettinck, K.; Vanrolleghem, P. A. Modelling of the crystallization kinetics of fats. *Trends Food Sci. Technol.* **2003**, *14*, 79−92.
(6) Wright, A. J.; Narine, S. S.; Marangoni, A. G. Comparison of experimental techniques used in lipid crystallization studies. *J. Am. Oil Chem. Soc.* **2000**, *77*, 1239−1242.
(7) Singh, A. P.; McClements, D. J.; Marangoni, A. G. Solid fat content determination by ultrasonic velocimetry. *Food Res. Int.* **2004**, *37*, 545−555.
(8) Foubert, I.; Vanrolleghem, P. A.; Dewettinck, K. A differential scanning calorimetry method to determine the isothermal crystallization kinetics of cocoa butter. *Thermochim. Acta* **2003**, *400*, 131−142.
(9) Hindle, S.; Povey, M. J. W.; Smith, K. Kinetics of crystallization in *n*-hexadecane and cocoa butter oil-in-water emulsions accounting for droplet collision-mediated nucleation. *J. Colloid Interface Sci.* **2000**, *232*, 370−380.
(10) Hindle, S. A.; Povey, M. J. W.; Smith, K. W. Characterizing cocoa-butter seed crystals by the oil-in-water emulsion crystallization method. *J. Am. Oil Chem. Soc.* **2002**, *79*, 993−1002.
(11) Gibon, V.; Durant, F.; Deroanne, C. β'-Stability of some pure triglycerides and blends studied by X-ray powder diffraction measurements. *An. Soc. Sci. Bruxelles* **1987**, *101*, 111−130.
(12) van Malssen, K.; Peschar, R.; Schenk, H. Real-time X-ray powder diffraction investigations on cocoa butter. I. Temperature-dependent crystallization behavior. *J. Am. Chem. Soc.* **1996**, *73*, 1209−1215.
(13) Rousset, P., Modeling crystallization kinetics of triacylglycerols. *Physical Properties of Lipids*; Marangoni, A. G., Narine, S. S., Eds.; Marcel Dekker: New York, 2002; pp 1−36.
(14) Avrami, M. Kinetics of phase change. I: General theory. *J. Chem. Phys.* **1939**, *7*, 1103−1112.
(15) Avrami, M. Kinetics of phase change. II: Transformation-time relations for random distribution of nuclei. *J. Chem. Phys.* **1940**, *8*, 212−224.
(16) Avrami, M. Kinetics of phase change. III: Granulation, phase change, and microstructures. *J. Chem. Phys.* **1941**, *9*, 177−184.
(17) Johnson, W.; Mehl, R. Reaction kinetics in processes of nucleation and growth. *Trans. Am. Inst. Min. Metall. Eng., Iron Steel Div.* **1939**, *135*, 416−46.
(18) Erofeev, B. V. *Compt. Rend. Acad. Sci. USSR* (*Dokl. Akad. Nauk SSSR*) **1946**, *52*, 511−514.
(19) Kolmogorov, A. A statistical theory for the recrystallization of metals. *Bull. Acad. Sci. USSR Mater. Sci.* (*Akad. Nauk SSSR, Izv., Ser. Matem.*) **1937**, *1*, 355−359.
(20) Kloek, W.; Walstra, P.; van Vliet, T. Crystallization kinetics of fully hydrogenated palm oil in sunflower oil mixtures. *J. Am. Oil Chem. Soc.* **2000**, *77*, 389−398.
(21) Foubert, I.; Vanrolleghem, P. A.; Vanhoutte, B.; Dewettinck, K. Dynamic mathematical model of the crystallization kinetics of fats. *Food Res. Int.* **2002**, *35*, 945−956.
(22) Toro-Vazquez, J.; Herrera-Coronado, V.; Dibildox-Alvarado, E.; Charo-Alonso, M.; Gomez-Aldapa, C. Induction time of crystallization in vegetable oils, comparative measurements by differential scanning calorimetry and diffusive light scattering. *J. Food Sci.* **2002**, *67*, 1057−1065.
(23) Metin, S.; Hartel, R. W. Thermal analysis of isothermal crystallization kinetics in blends of cocoa butter with milk fat or milk fat fractions. *J. Am. Oil Chem. Soc.* **1998**, *75*, 1617−1624.
(24) Kerti, K. Investigating isothermal DSC method to distinguish between cocoa butter and cocoa butter alternatives. *J. Therm. Anal. Calorim.* **2000**, *63*, 205−219.
(25) Hatakeyama, T.; Quinn, F. X. DSC-thermal analysis and kinetics of cocoa butter crystallization. *Thermal Analysis: Fundamentals and Applications to Polymer Science*, Wiley: Chichester, U.K., 1997; 68−485.
(26) Vyazovkin, S.; Sbirrazzuoli, N. Isoconversional analysis of calorimetric data on nonisothermal crystallization of a polymer melt. *J. Phys. Chem. B* **2003**, *107*, 882−888.
(27) Serra, R.; Sempere, J.; Nomen, R. A new method for the kinetic study of thermoanalytical data: The non-parametric kinetics method. *Thermochim. Acta* **1998**, *316*, 37−45.
(28) Serra, R.; Nomen, R.; Sempere, J. The non-parametric kinetics. *J. Therm. Anal.* **1998**, *52*, 933−943.
(29) Khanna, Y. P.; Taylor, T. J. Comments and recommendations on the use of the Avrami equation for physico-chemical kinetics. *Polym. Eng. Sci.* **1988**, *28*, 1042−1045.
(30) Kissinger, H. E. Reaction kinetics in differential thermal analysis. *Anal. Chem.* **1957**, *29*, 1702−1706.
(31) Ozawa, T. A quick, direct method for the determination of activation energy from thermogravimetric data. *Bull. Chem. Soc. Jpn.* **1965**, *38*, 1881−1886.
(32) Flynn, J. H.; Wall, L. A. A quick, direct method for the determination of activation energy from thermogravimetric data. *J. Polym. Sci., Part C: Polym. Lett.* **1966**, *4*, 323−328.
(33) Kaiser, M.; Ticmanis, U. Thermal stability of diazodinitrophenol. *Thermochim. Acta* **1995**, *250*, 137−149.
(34) Vyazovkin, S. Is the Kissinger equation applicable to the processes that occur on cooling? *Macromol. Rapid Commun.* **2002**, *23*, 771−775.
(35) Mullin, J. W. *Crystallization*, 4th ed., Butterworth−Heinemann: Oxford, U.K., 2001.
(36) Friedman, H. L. Kinetics of thermal degradation of char-forming plastics from thermogravimetry. Application to a phenolic plastic. *J. Polym. Sci., Part C: Polym. Lett.* **1965**, *6*, 183−195.
(37) Vyazovkin, S. Evaluation of activation energy of thermally stimulated solid-state reactions under arbitrary variation of temperature. *J. Comput. Chem.* **1997**, *18*, 393−402.
(38) Vyazovkin, S.; Dollimore, D. Linear and nonlinear procedures in isoconversional computations of the activation energy of nonisothermal reactions in solids. *J. Chem. Info. Comput. Sci.* **1996**, *36*, 42−45.
(39) Li, C. R.; Tang, T. B. A new method for analysing non-isothermal thermoanalytical data from solid-state reactions. *Thermochim Acta* **1999**, *325*, 43−46.
(40) Li, C. R.; Tang, T. B. Isoconversional method for kinetic analysis of solid-state reactions from dynamic thermoanalytical data. *J. Mater. Sci.* **1999**, *34*, 3467−3470.
(41) Telleria, I.; Barandiarán, J. M. Kinetics of the primary, eutectic, and polymorphic crystallization of metallic glasses studied by continuous scan methods. *Thermochim. Acta* **1996**, *280*/*281*, 279−287.
(42) Mazzobre, M. F.; Soto, G.; Aguilera, J. M.; Beura, M. P. Crystallization kinetics of lactose in systems co-lyofilized with trehalose. Analysis by differential scanning calorimetry. *Food Res. Int.* **2001**, *34*, 903−911.
(43) Koster, U.; Meinhardt, J. Crystallization of highly undercooled metallic melts and metallic glasses around the glass transition temperature. *Mater. Sci. Eng., A* **1994**, *178*, 271−278.
(44) Koster, U.; Meinhardt, J.; Roos, S.; Busch, R. Formation of quasicrystals in bulk glass forming Zr−Cu−Ni−Al alloys. *Mater. Sci. Eng., A* **1997**, *226*, 995−998.
(45) Šesták, J.; Berggren, G. Mechanical properties of fats in relation to their crystallization. *Thermochim. Acta* **1971**, *3*, 1−398.
(46) Malek, J.; Criado, J. M. Is the Šesták−Berggren equation a general expression of kinetic models. *Thermochim. Acta* **1991**, *175*, 305−309.
(47) Vanhoutte, B.; Dewettinck, K.; Foubert, I.; Vanlerberghe, B.; Huyghebaert, A. The effect of phospholipids and water on the isothermal crystallisation of milk fat. *Eur. J. Lipid Sci. Technol.* **2002**, *104*, 490−495.
(48) Karkanas, P. I.; Partridge, I. K.; Attwood, D. Modelling the cure of a commercial epoxy resin for applications in resin transfer moulding. *Polym. Int.* **1996**, *41*, 183−191.
(49) Karkanas, P. I.; Partridge, I. K. Cure modeling and monitoring of epoxy/amine resin systems. I. Cure kinetics modeling. *J. Appl. Polym. Sci.* **2000**, *77*, 1419−1431.
(50) Kamal, M. R. Thermoset characterization for moldability analysis. *Polym. Eng. Sci.* **1974**, *14*, 231−239.

(51) Sewry, J. D.; Brown, M. E. Model-free kinetic analysis? *Thermochim. Acta* **2002**, *101*, 217−225.
(52) Press, W. H.; Flannery, B. P.; Teukolsky, S. A.; Vetterling, W. T. *Numerical Recipes in Pascal, The Art of Scientific Computing*, Cambridge University Press: Cambridge, U.K., 1989.
(53) Wesdorp, L. H. Liquid-Multiple Solid-Phase Equilibria in Fats−Theory and Experiments. Ph.D. Thesis. Delft University of Technology: The Netherlands, 1990.
(54) Sato, K.; Arishima, T.; Wang, Z. H.; Ojima, K.; Sagi, N.; Mori, H. Polymorphism of POP and SOS. I. Occurrence and polymorphic transformation. *J. Am. Oil Chem. Soc.* **1989**, *66*, 664−674.
(55) Hiemenz, P. C. *Polymer Chemistry: The Basic Concepts*, Marcel Dekker: New York, 1984; p 219.
(56) Cebula, D. J.; Smith, K. W. Differential scanning calorimetry of confectionery fats. Pure triglycerides: Effect of cooling and heating rate variation. *J. Am. Oil Chem. Soc.* **1991**, *68*, 591−595.

Received for review November 23, 2004. Revised manuscript received February 17, 2005. Accepted February 24, 2005.

JF048036O